

Monolithic integration of a nanomechanical resonator to an optical microdisk cavity

Onur Basarir,^{1,2} Suraj Bramhavar,¹ and Kamil L. Ekinci^{1,*}

¹College of Engineering and the Photonics Center, Boston University, Boston, Massachusetts, 02215, USA

²Present address : Fakultät für Physik and Center for NanoScience, Ludwig-Maximilians-Universität, Geschwister-Scholl-Platz 1, 80539 München, Germany

*ekinci@bu.edu

Abstract: We report a Silicon nano-opto-mechanical device in which a nanomechanical doubly-clamped beam resonator is integrated to an optical microdisk cavity. Small flexural oscillations of the beam cause intensity modulations in the circulating optical field in the nearby microdisk cavity. By monitoring the corresponding fluctuations in the cavity transmission via a fiber-taper, one can detect these oscillations with a displacement sensitivity approaching $10 \text{ fm}\cdot\text{Hz}^{-1/2}$ at an input power level of $50 \mu\text{W}$. Both the in-plane and out-of-plane fundamental flexural resonances of the beam can be read out by this approach — the latter being detectable due to broken planar symmetry in the system. Access to multiple mechanical modes of the same resonator may be useful in some applications and may enable interesting fundamental studies.

© 2012 Optical Society of America

OCIS codes: (120.4880) Optomechanics; 120.7280 (Vibration analysis); (230.3990) Micro-optical devices.

References and links

1. K. L. Ekinci and M. L. Roukes, "Nanoelectromechanical systems," *Rev. Sci. Instrum.* **76**, 061101 (2005).
2. H. G. Craighead, "Nanoelectromechanical systems," *Science* **290**, 1532–1535 (2000).
3. J. Lawall and E. Kessler, "Michelson interferometry with 10 pm accuracy," *Rev. Sci. Instrum.* **71**, 2669–2676 (2000).
4. T. Kouh, D. Karabacak, D. H. Kim, and K. L. Ekinci, "Diffraction effects in optical interferometric displacement detection in nanoelectromechanical systems," *Appl. Phys. Lett.* **86**, 013106 (2005).
5. A. Xuereb, R. Schnabel, and K. Hammerer, "Dissipative optomechanics in a michelson-sagnac interferometer," *Phys. Rev. Lett.* **107**, 213604 (2011).
6. C. M. Hernandez, T. W. Murray, and S. Krishnaswamy, "Photoacoustic characterization of the mechanical properties of thin films," *Appl. Phys. Lett.* **80**, 691–693 (2002).
7. A. Sampathkumar, T. W. Murray, and K. L. Ekinci, "Photothermal operation of high frequency nanoelectromechanical systems," *Appl. Phys. Lett.* **88**, 223104 (2006).
8. O. Arcizet, P.-F. Cohadon, T. Briant, M. Pinard, and A. Heidmann, "Radiation-pressure cooling and optomechanical instability of a micromirror," *Nature* **444**, 71–74 (2006).
9. D. Kleckner and D. Bouwmeester, "Sub-kelvin optical cooling of a micromechanical resonator," *Nature* **444**, 75–78 (2006).
10. J. D. Thompson, B. M. Zwickl, A. M. Jayich, F. Marquardt, S. M. Girvin, and J. G. E. Harris, "Strong dispersive coupling of a high-finesse cavity to a micromechanical membrane," *Nature* **452**, 72–75 (2008).
11. S. Groblacher, K. Hammerer, M. R. Vanner, and M. Aspelmeyer, "Observation of strong coupling between a micromechanical resonator and an optical cavity field," *Nature* **460**, 724–727 (2009).

12. I. Favero, S. Stappfner, D. Hunger, P. Paulitschke, J. Reichel, H. Lorenz, E. M. Weig, and K. Karrai, "Fluctuating nanomechanical system in a high finesse optical microcavity," *Opt. Express* **17**, 12813–12820 (2009).
13. D. W. Carr, S. Evoy, L. Sekaric, H. G. Craighead, and J. M. Parpia, "Measurement of mechanical resonance and losses in nanometer scale silicon wires," *Appl. Phys. Lett.* **75**, 920–922 (1999).
14. D. Karabacak, T. Kouh, and K. L. Ekinci, "Analysis of optical interferometric displacement detection in nanoelectromechanical systems," *J. Appl. Phys.* **98**, 124309 (2005).
15. I. D. Vlamincik, J. Roels, D. Taillaert, D. V. Thourhout, R. Baets, L. Lagae, and G. Borghs, "Detection of nanomechanical motion by evanescent light wave coupling," *Appl. Phys. Lett.* **90**, 233116 (2007).
16. M. Li, W. H. P. Pernice, C. Xiong, T. Baehr-Jones, M. Hochberg, and H. X. Tang, "Harnessing optical forces in integrated photonic circuits," *Nature* **456**, 480–484 (2008).
17. J. Roels, I. De Vlamincik, L. Lagae, B. Maes, D. Van Thourhout, and R. Baets, "Tunable optical forces between nanophotonic waveguides," *Nature Nanotech.* **4**, 510–513 (2009).
18. O. Basarir, S. Bramhavar, G. Basilio-Sanchez, T. Morse, and K. L. Ekinci, "Sensitive micromechanical displacement detection by scattering evanescent optical waves," *Opt. Lett.* **35**, 1792–1794 (2010).
19. O. Basarir, S. Bramhavar, and K. L. Ekinci, "Near-field optical transducer for nanomechanical resonators," *Appl. Phys. Lett.* **97**, 253114 (2010).
20. T. J. Kippenberg and K. J. Vahala, "Cavity optomechanics: Back-action at the mesoscale," *Science* **321**, 1172–1176 (2008).
21. M. Eichenfield, R. Camacho, J. Chan, K. J. Vahala, and O. Painter, "A picogram- and nanometre-scale photonic-crystal optomechanical cavity," *Nature* **459**, 550–555 (2009).
22. M. Li, W. H. P. Pernice, and H. X. Tang, "Reactive cavity optical force on microdisk-coupled nanomechanical beam waveguides," *Phys. Rev. Lett.* **103**, 223901 (2009).
23. Q. Lin, J. Rosenberg, X. Jiang, K. J. Vahala, and O. Painter, "Mechanical oscillation and cooling actuated by the optical gradient force," *Phys. Rev. Lett.* **103**, 103601 (2009).
24. K. Srinivasan, H. Miao, M. T. Rakher, M. Davanco, and V. Aksyuk, "Optomechanical transduction of an integrated silicon cantilever probe using a microdisk resonator," *Nano Letters* **11**, 791–797 (2011).
25. G. Anetsberger, O. Arcizet, Q. P. Unterreithmeier, R. Riviere, A. Schliesser, E. M. Weig, J. P. Kotthaus, and T. J. Kippenberg, "Near-field cavity optomechanics with nanomechanical oscillators," *Nature Phys.* **5**, 909–914 (2009).
26. G. S. Wiederhecker, L. Chen, A. Gondarenko, and M. Lipson, "Controlling photonic structures using optical forces," *Nature* **462**, 633–636 (2009).

1. Introduction

A nanomechanical resonator [1, 2] stores energy in its mechanical oscillations. Small perturbations to the resonator typically result in large changes in the amplitude or frequency of these oscillations. By monitoring these nanomechanical oscillations, one can devise a sensitive probe of both external signals and phenomena intrinsic to the resonator. Detecting the exceedingly small motion of a nanomechanical resonator with high sensitivity, therefore, remains an overarching theme in research involving nanomechanical resonators.

Far field optical techniques provide remarkable sensitivity in displacement (motion) detection [3]. Using a typical path-stabilized Michelson interferometer [4–6], for instance, one can easily obtain a displacement sensitivity of $\sim 100 \text{ fm} \cdot \text{Hz}^{-1/2}$ at $100\text{-}\mu\text{W}$ -level optical powers. However, this sensitivity is degraded as the device size approaches or becomes smaller than the diffraction limited optical probe spot [7]. As the moving structure becomes smaller, light is reflected back inefficiently, resulting in a sensitivity loss. Similarly, a Fabry-Perot interferometer can provide very high sensitivity. Impressive displacement sensitivities well below $100 \text{ fm} \cdot \text{Hz}^{-1/2}$ have been reported on microelectromechanical systems (MEMS) devices [8–12]. However, as above, the moving mirror must be larger than the optical spot size so that one can create a high-finesse cavity. As the device size approaches the wavelength of light, sensitivities of conventional Fabry-Perot interferometers decrease dramatically – due to diffraction and optical losses. A good example to the point is the Fabry-Perot cavity created between the top surface of a nanomechanical beam and a substrate underneath [13]. While this provides a usable cavity for nanomechanical displacement detection, the low cavity finesse [14] results in degraded displacement sensitivity.

Near-field (evanescent) optical interactions offer viable approaches for sensitive motion de-

tection beyond the diffraction limit with less stringent coherence and stability requirements. In the nanomechanical domain, sensitive motion sensing using direct evanescent coupling and scattering [15–19] has recently been realized. More sensitivity can be obtained by coupling the nanomechanical motion to an optical cavity at the subwavelength scale. Recent efforts along this line have resulted in the active field of cavity optomechanics [20]. Several different devices, in which a nanomechanical resonator is coupled to photonic crystal [21], microdisk [22–24], microtoroid [25] and microring [26] cavities, have successfully been demonstrated.

In this manuscript, we report the design, fabrication and operation of a novel nano-optomechanical device, in which a nanomechanical doubly-clamped beam resonator is integrated to an optical microdisk cavity. This device obviates the need for alignment of the mechanical resonator to the optical cavity. Furthermore, broken planar symmetry of the system during the fabrication process enables us to observe the out-of-plane flexural motion of the mechanical resonator — in addition to the expected in-plane motion. In section 2, we discuss the novel aspects of the device along with a brief description of the fabrication. The experimental set up and the results from measurements are discussed in sections 3 and 4, respectively. Finally, conclusions are presented in the last section.

2. Device design and fabrication

A scanning electron microscope (SEM) image of one of our devices is shown in Fig. 1(a). Here, a nanomechanical doubly-clamped beam is co-fabricated on a chip with a microdisk structure. The illustration in Fig. 1(b) displays the cross-sectional view of the device at the $x_1 - x_3$ plane at the center of the beam. All the microdisks in this study have the same diameter of $40\ \mu\text{m}$. The thickness t of the beam and the microdisk are determined by the thickness of the Silicon layer and $t = 230\ \text{nm}$. The width w of the beam and the gap values x_1^e between the beam and the microdisk are set in the fabrication process. In equilibrium, there is a small bending in the beam, which breaks the symmetry by offsetting the center of the beam in the x_3 direction to an equilibrium position x_3^e (see below for a detailed discussion of x_3^e). In this study, we have kept the beam width at $w = 250\ \text{nm}$ and varied the gap as $x_1^e = 150, 250$ and $350\ \text{nm}$. We have also varied the beam lengths l as $l = 7, 10, 12$ and $15\ \mu\text{m}$. Given the three different x_1^e and four different l values, we have collected data on a total of 12 different resonators. The optical coupling to the device is accomplished by bringing a separate fiber-taper into the vicinity of the cavity as described below.

Two devices that are quite similar to our device in design have recently been reported. We now compare our device to these and describe the differences where appropriate. The first device that appears to be similar to ours is described in [22]. There, a nanomechanical beam resonator, which serves both as the mechanical element and the input-output coupler to a microdisk resonator, is fabricated next to the microdisk structure. The optical coupling to the nanomechanical waveguide is accomplished by two grating couplers with 10% efficiency each. In our design, the nanomechanical beam is independent from the rest of the elements on the chip, and the light is coupled into and out of the microdisk through a fiber-taper waveguide. The fiber-taper obviates the need for the inefficient grating couplers. The fact that the nanomechanical beam need not have traveling optical modes in our design allows us to change the linear dimensions of the nanomechanical beam arbitrarily. A second similar device is described in [24]. Here, the mechanical resonator has a curved geometry while the optical coupling method is identical to ours. The curved geometry, while interesting, comes with some complexities. For instance, the geometry sets some hard limits on the resonator dimensions and hence its mechanical parameters. Scaling this device down in size and up in frequency appears challenging because the mechanical element must be wrapped around the disk. In contrast, in our simple linear geometry, one can simply reduce the length of the beam or make the beam wider.

To fabricate our devices, we use a Silicon-on-Insulator (SOI) wafer, which has a 500 nm Si device layer on top of a 3 μm SiO_2 layer. As a first step, a thermal oxide is grown in the Silicon layer in order to reduce the thickness of the Silicon layer by a wet etch. Next, electron beam lithography is performed to define a metal mask. The mask pattern is transferred into the Silicon by an anisotropic dry etch in a reactive ion etcher (RIE). The metal mask is then removed. Normally, at this step one can release the beams and complete the fabrication process. However, in our case, we define *mesa* structures in order to isolate the devices from the rest of the chip for efficient optical coupling using a fiber-taper. For the purpose of fabricating the mesa structures, we perform a photolithography step followed by deep-RIE. The final step is the release of the suspended structures in an HF vapor etcher.

3. Experimental set up

A schematic of our measurement setup is superimposed on the SEM image of a device in Fig. 1(a). A fiber-taper is used for coupling light into and out of the microdisk resonator. The tapered region has a diameter of $d \approx 1 \mu\text{m}$. The device chip is mounted onto a piezostage (for positioning with respect to the tapered waveguide) in a vacuum chamber with a base pressure of 2×10^{-2} Pa. A tunable diode laser operating in the telecom band is used for probing the devices. The light coming from the laser passes through the fiber-taper, interacts with the microdisk and is directed onto a high-speed photodetector. A fiber polarization controller is used for selectively exciting transverse electric (TE) and transverse magnetic (TM) whispering gallery mode (WGM) resonances of the microdisk. The transmission profile is monitored with a multimeter; a radio-frequency (rf) spectrum analyzer is used for mechanical measurements.

When the microdisk is driven close to one of its WGM resonances, the mechanical oscillations of the doubly-clamped beam induce modulations in the optical field circulating around the microdisk through local optical index changes. Thus, the mechanical signals are embedded in the cavity transmission T and can be detected by monitoring the rf spectrum of T . For small oscillations of the nanomechanical resonator at the limit $\kappa \gg \Omega_m$ (κ is the cavity linewidth and Ω_m is the mechanical resonance frequency), the optical power P^{out} incident on the photodetector can be expressed as [23]

$$P^{out}(t) \approx P^{in} \left[T + \left. \frac{\partial T}{\partial \omega} \right|_{\omega=\omega_d} g_i \delta x_i(t) \right]. \quad (1)$$

In this expression, P^{in} is the incident power on the waveguide; the transmission T and the derivative $|\partial T/\partial \omega|$ are evaluated at the optical detection frequency ω_d ; $\delta x_i(t)$ is the small time-dependent oscillation amplitude of the mechanical resonator in the i direction ($i = 1, 3$). $g_i = \partial \omega_o / \partial x_i$ is the optomechanical coupling coefficient, where ω_o is the optical resonance frequency and x_i is the time-dependent position of the mechanical device.

4. Measurements

Figure 1(c) shows the normalized transmission spectrum of a 40- μm -diameter microdisk coupled to a doubly-clamped beam ($l \times w \times t = 12 \mu\text{m} \times 250 \text{ nm} \times 230 \text{ nm}$) as a function of detection wavelength. The beam and microdisk are separated by a nominal equilibrium gap fabricated to be $x_1^e \approx 250 \text{ nm}$. The optical transmission spectrum is optimized in the $x_1 - x_3$ plane for TM polarization in the under-coupled regime by changing the position of the fiber-taper with respect to the microdisk. Several dips corresponding to optical modes with different radial and azimuthal numbers can be observed. Each displays a Lorentzian lineshape. A representative mode with optical resonance at a wavelength of 1577.1 nm and optical quality factor

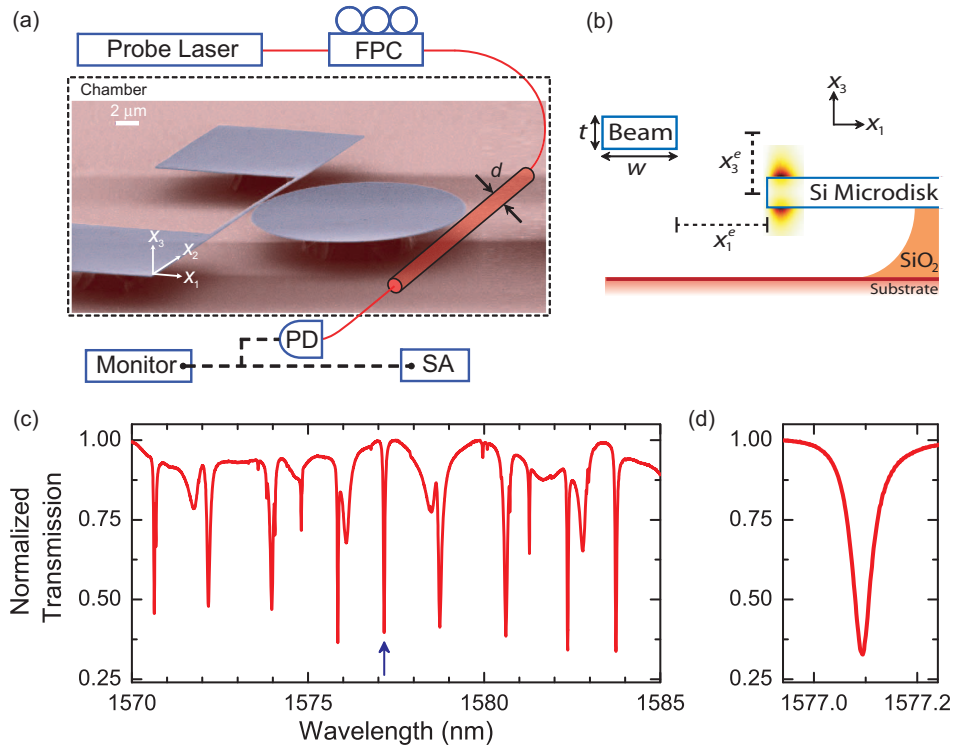


Fig. 1. (a) Schematic of the experimental setup superimposed on the SEM image of a doubly-clamped beam resonator coupled to a microdisk. The linear dimensions of the beam are $l \times w \times t = 15 \mu\text{m} \times 250 \text{nm} \times 230 \text{nm}$ and the disk diameter is $20 \mu\text{m}$. Light from a diode laser is directed into the fiber-taper waveguide and then sent onto a high-speed photodetector (PD). A fiber polarization controller (FPC) is used in order to selectively excite optical modes and a spectrum analyzer (SA) is used for noise measurements. (b) Cross-sectional view of the device through the center of the beam in the $x_1 - x_3$ plane. The optical mode is localized near the microdisk perimeter as shown in the simulation. Note the small offset x_3^e in the x_3 direction. (c) Normalized optical transmission T optimized for TM polarization of a $40\text{-}\mu\text{m}$ -diameter microdisk coupled to a $(l \times w \times t = 12 \mu\text{m} \times 250 \text{nm} \times 230 \text{nm})$ doubly clamped beam. (d) Zoomed-in spectrum of a TM mode with a quality factor of $Q_o \approx 35,000$.

$Q_o \approx 35,000$ is shown in Fig. 1(d). The lower effective index of TM modes increases the mode matching between the waveguide and the microdisk, thus offering better coupling.

Thermal-mechanical oscillations of the NEMS resonator can be detected by exciting the cavity at a single wavelength close to its resonance and monitoring the spectrum of T . Figure 2(a) displays the high-frequency spectrum of the transmission, measured using the optical cavity mode shown in Fig. 1(d). For this measurement, the cavity is driven at one of its maximum sensitivity points, $\lambda_d \approx 1577.08 \text{nm}$, with an input power of $P^{in} \approx 50 \mu\text{W}$. Two well-separated thermal peaks are observed at 5.55MHz and 10.31MHz , corresponding to the fundamental flexural modes of the mechanical resonator in the x_3 (out-of-plane) and x_1 (in-plane) directions, respectively. Both peaks can be fit by Lorentzians with mechanical quality factors of $Q_m \approx 1,300$. Independent measurements on the resonator using a Michelson interferometer

confirm the frequency of the out-of-plane mode.

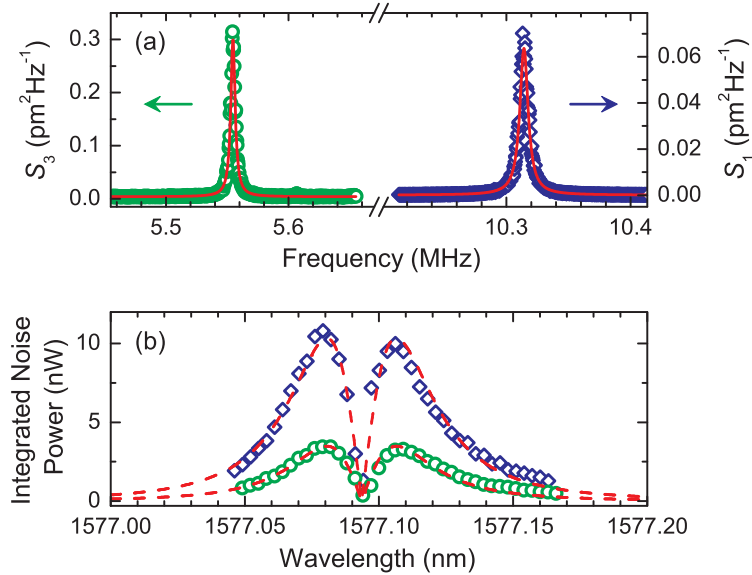


Fig. 2. (a) Thermal noise peaks of a doubly-clamped beam resonator ($l \times w \times t = 12 \mu\text{m} \times 250 \text{ nm} \times 230 \text{ nm}$) measured in vacuum with a probe power of $P^{in} \approx 50 \mu\text{W}$. The low frequency peak is the out-of-plane mode and the high frequency peak is the in-plane mode. (b) Integrated optical noise powers of the in-plane (diamonds) and out-of-plane (circles) mode as a function of the probe wavelength.

A fully planar device, where the nanomechanical resonator lies on the same plane as the microdisk [$x_1 - x_2$ plane in Fig. 1(a)], should exhibit strong optomechanical coupling g_1 only in the x_1 direction; the out-of-plane coupling g_3 in the x_3 direction should be zero due to the symmetry if the device is truly planar [25]. The modes observed in Fig. 2(a) in the x_1 and x_3 directions with comparable strengths are most likely a consequence of the slight bending of the beams during fabrication, which is also noticeable in high-magnification high-tilt SEM images. This bending breaks the symmetry by offsetting the center of the beam in the x_3 direction to an equilibrium position x_3^e . Hence, the oscillations of the mechanical resonator in the x_3 direction can modulate the local dielectric index of the cavity, giving rise to a non-zero optomechanical coupling in the x_3 direction. We provide a more detailed discussion of this unexpected phenomenon below.

We now describe the displacement calibration. The measured signals can be converted into displacements by considering the rms thermal amplitude of the mode $\langle(\delta x_i)^2\rangle^{1/2}$ at temperature θ [17]: $\langle(\delta x_i)^2\rangle = k_B\theta/k_i$, where k_B is the Boltzmann constant. The mode stiffnesses k_i can be found using device geometry and material properties. For the in-plane mode, $k_1 \approx 5 \text{ N}\cdot\text{m}^{-1}$, and for the out-of-plane mode, $k_3 \approx 2 \text{ N}\cdot\text{m}^{-1}$. With $\theta = 300 \text{ K}$ [19], one obtains rms amplitudes of $\langle(\delta x_1)^2\rangle^{1/2} \approx 28 \text{ pm}$ and $\langle(\delta x_3)^2\rangle^{1/2} \approx 45 \text{ pm}$. Using this calibration, the displacement sensitivities (noise floors) are found to be $\sqrt{S_1} \approx 9 \text{ fm}\cdot\text{Hz}^{-1/2}$ and $\sqrt{S_3} \approx 59 \text{ fm}\cdot\text{Hz}^{-1/2}$.

Thermal noise measurements can be used to determine the optomechanical coupling coefficients g_i . Returning to Eq. (1), we notice that the thermal oscillations of the i^{th} mechanical mode result in a total (integrated) optical noise power $P_i^{out} \approx P_i^{in} g_i \left. \frac{\partial T}{\partial \omega} \right|_{\omega=\omega_d} \langle(\delta x_i)^2\rangle^{1/2}$. Fig-

Figure 2(b) shows the measured noise powers P_1^{out} and P_3^{out} for the in-plane (diamonds) and out-of-plane (circles) mechanical modes. The dashed lines are best fits using the available P_i^{out} , P_i^{in} , $|\partial T/\partial \omega|$ and $\langle (\delta x_i)^2 \rangle^{1/2}$, with the fit parameters being the optomechanical coupling coefficients g_i . Thus, g_i are found as $g_1/2\pi \approx 46$ MHz/nm for in-plane motion and $g_3/2\pi \approx 10$ MHz/nm for out-of-plane motion. Furthermore, we have not observed dissipative coupling and believe that the mechanical resonator couples only dispersively to the microcavity.

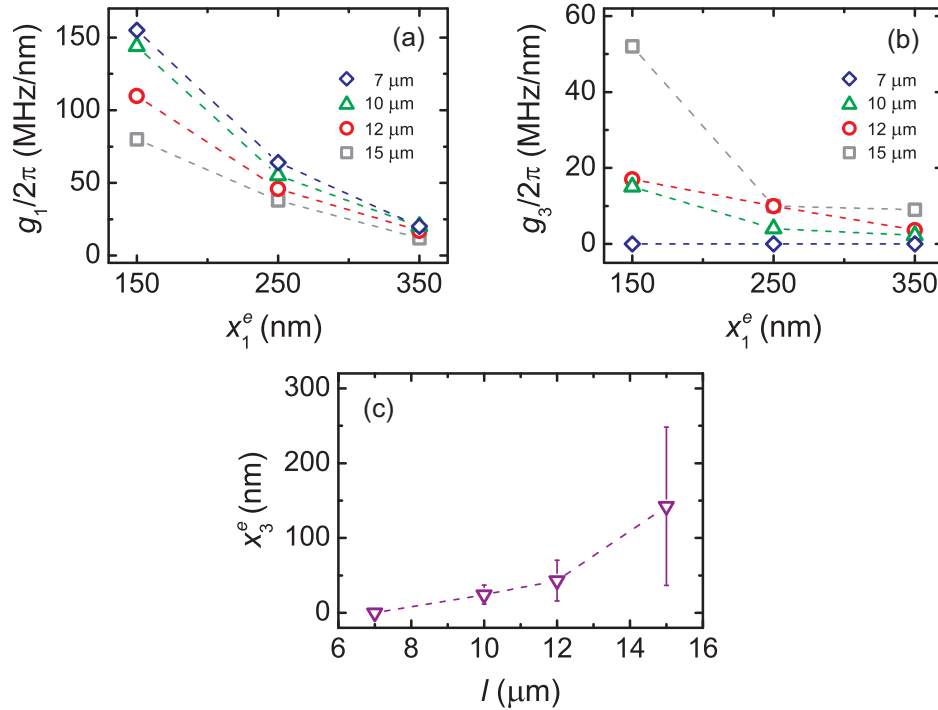


Fig. 3. (a) $g_1/2\pi$ and (b) $g_3/2\pi$ as a function of x_1^e for beams having different lengths. (c) Calculated x_3^e as a function of beam length l . Each data point is obtained from an average over four devices with the same l but different x_1^e values.

In order to understand the effects of device dimensions on optomechanical coupling, we have repeated the above-described measurements on devices with a range of linear dimensions and nominal gap values. In particular, we have changed both the lengths l of the doubly-clamped beams and the equilibrium gaps x_1^e while keeping the diameter of the microdisks fixed at $40 \mu\text{m}$. Four different length values ($l = 7, 10, 12$ and $15 \mu\text{m}$), and three different gap values ($x_1^e = 150, 250$ and 350 nm) are used, resulting in 12 resonators with equal thicknesses ($t = 230$ nm) and widths ($w = 250$ nm). In Fig. 3(a) and (b), we respectively display the experimentally obtained $g_1/2\pi$ and $g_3/2\pi$ for each beam as a function of x_1^e . Both g_1 and g_3 tend to increase as x_1^e gets smaller due to stronger field gradients in the vicinity of the microdisk. For the in-plane mode, the shorter the beam, the larger the g_1 at any given x_1^e . However, the situation changes for the out-of-plane coupling: longer beams exhibit larger g_3 . For the shortest beam ($l = 7 \mu\text{m}$), $g_3 \approx 0$.

As noted above, the out-of-plane coupling can be explained by a small bending in the beams, which displaces their centers in the out-of-plane direction, resulting in symmetry breaking. This small equilibrium displacement in the out-of-plane direction is shown as x_3^e in Fig. 1(b). Stiffer

shorter beams are not expected to undergo significant bending, thus resulting in small g_3 as observed in the experiments. To gain more insight, we can estimate the vertical offset x_3^e for each device using a perturbative method [25]. These estimates of x_3^e obtained for each device are shown in Fig. 3(c). These estimates are obtained as follows. The presence of a dielectric mechanical resonator perturbs the energy in the cavity, providing the optomechanical coupling. We first determine g_3 for each device from the experiments as outlined above. Next, we calculate the energy change in the cavity using g_3 along with calculated optical mode volumes, evanescent decay lengths and overlap integrals. Finally, we extract the x_3^e value, which is necessary for such a coupling to occur. The results are consistent with the earlier assumption that longer softer beams have larger offset values x_3^e , whereas $x_3^e \approx 0$ for shorter beams. The large error bar for the longest beam ($l = 15 \mu\text{m}$) may be due to undercuts for the particular device, changing its k_3 from the estimated value and causing excess bending.

5. Discussion and conclusions

Our device design, which allows the measurement of both in-plane and out-of-plane mechanical oscillations of a doubly-clamped nanomechanical beam with high displacement sensitivity, could provide a unique platform for sensing applications and fundamental studies. From a fundamental physics point of view, one could investigate the intermodal coupling between the in-plane and out-of-plane modes. By increasing the circulating light intensity in the cavity, it might be possible to observe a strong coupling between these two mechanical modes. In that case, one could further tune the individual resonance frequencies by changing the intensity of the incident light. As a result, one could observe a power transfer and accomplish adiabatic and diabatic transition process between these modes based on optical forces. In mass sensing applications, the straightforward access to the two mechanical modes in a device such as ours might allow accurate mass and position measurements for the attached mass. Other sensing application including force sensing could also benefit from similar approaches.

The device here could be improved by using smaller diameter cavities, which would allow for a stronger optomechanical coupling due to the reduced optical mode volume. Microdisk cavities could be deformed into racetrack resonators with the nanomechanical beam residing along the linear side, resulting in an enhanced coupling. The stability of this design could further be increased by anchoring the fiber-taper onto fixed supports. By simply introducing an additional intensity modulated laser in a pump-probe scheme, one could excite the mechanical modes via optical gradient forces and attain large amplitude responses.

Acknowledgements

The authors acknowledge support from the U.S. National Science Foundation (NSF) through Grants ECCS-0643178, CBET-0755927 and CMMI-0970071. O.B. was partially supported by a Boston University Photonics Center Fellowship.